17th World Conference on Earthquake Engineering, 17WCEE
Sendai, Japan - September 13th to 18th 2020

QUANTIFICATION OF EFFECTS OF SINGLE AND COMPLEX 3D-TOPOGRAPHY ON GROUND MOTION CHARACTERISTICS

Vishal [1], J.P. Narayan [2]

[1] *Research Scholar, Department of Earthquake Engineering, Indian Institute of Technology Roorkee-247667, INDIA, email: vishal@eq.iitr.ac.in*
[2] *Professor, Department of Earthquake Engineering, Indian Institute of Technology Roorkee-247667, INDIA, email: jp.narayan@eq.iitr.ac.in*

Abstract

This paper presents the analysis of simulated responses of single and complex 3D conical topography models excited with simple wavelet in the quest of finding the answer why the numerically computed topography amplification on ground motion are lesser than those predicted experimentally. The responses have been estimated with azimuthal coverage of receivers to know the effect of receiver plane on amplification pattern. The complexity in the model is increased by increasing the number of sub-ridges and sub-valleys in the reference topography model. The SH- and SV-wave responses of 2D section of the conical topography are also computed and analysed. Fourth-order viscoelastic staggered-grid finite-difference programs are used for the simulation of seismic responses of various considered 3D- and 2D-topography models. The analysis of the 2D and 3D responses of the conical simple and complex topography revealed very large spectral amplifications and ASA in the 3D response as compared to the 2D response. It is inferred that there is no need of incorporation of topography effect in seismic hazard prediction on a hill with shape-ratio less than 0.15. The complexity of the conical ridge has caused unexpected amplification at the top of side-sub-ridges as compared to the central-sub-ridge. The obtained larger topography amplification using SSR method may be due to the de-amplification at/near the base of ridge. A considerable variation of topography amplification with azimuth is obtained at a particular elevation. Finally, it concluded that there is need of consideration of shape, azimuth, complexity and weathering of 3D topography as well as hypo-central distance and focal mechanism of earthquake in numerical estimates of the topography effects on ground motion characteristics.

Keywords: Viscoelastic finite difference simulation; 3D topography effect; Comparison between 2D and 3D effects.

1. Introduction

Hill topography is known to affect earthquake ground motions in the form of amplification of ground motion on hills/ridges and de-amplification in canyons/valleys with respect to a similar site on a flat terrain [1, 2, 3, 4, 5, 6]. The increase in population in hilly regions leads to construction of buildings, bridges, dams and hydro-power plants. These structures can be exposed to non-uniform ground motions due to topography effects. There are many cases where unusual high peak ground accelerations were observed on the top of a hill topography [2, 7, 8, 9]. The review of literature on the topography effects reveals that in most of the previous numerical studies simple 2D homogeneous triangular, semi-sine, semi-circular, trapezoidal, semi-elliptical etc. shaped topography were considered and maximum topographic spectral amplifications of the order of 2.5 were being reported [1,5,10,11]. In contrast to this, the experimental studies show spectral amplifications greater than 10 based on the earthquake records [11]. The possible reasons behind this mismatch can be the consideration of simple 2D section of topography and non-consideration of complex geometry and ridge-weathering. Lee et al. [12] observed that 3D shape of topography, source for excitation of model, frequency bandwidth and direction of incident seismic waves have a significant influence on spatial spectral amplifications [13]. But, there are limited theoretical studies considering simple and complex topography with different shape, shape ratio, weathering and azimuth of the receivers (shape ratio is defined as the ratio of height of ridge to its half-width at base).

The main contribution of this research work is the simulation of 2D (in a plane) and 3D responses of conical ridge topography with different shape-ratio and complexity for comparative 2D and 3D estimates of topography effects on ground motion characteristics as well as inferring the reason behind mismatch between the theoretically computed topography effects and the experimentally obtained one. The snapshots of the seismic wave-field are also computed to infer the behaviour of incident simple wave front after complex interaction with the 3D conical topography. The variation of conical topography effects with azimuth and elevation of the receiver points is also studied. The standard spectral ratio (SSR) method is used to compute the topography effects considering the record at the base as a reference ground motion.

2. Topography model, source-receiver arrays and parameters

2.1 Geometry of 3D conical ridge

To study the effects of shape-ratio and complexity of conical ridge on ground motion characteristics, the seismic response of the conical ridge models for the different shape-ratio and complex geometry have been computed. Fig.1a shows the sketch for the 3D-conical ridge model. The axis of ridge is considered as a reference point for the measurement of horizontal distances. The shape-ratio of the ridges has been varied by varying the height and keeping diameter of conical ridge constant (shape-ratio of conical ridge is simply the ratio of height to its radius). The diameter of the conical ridge is taken as 1000 m. The height of considered CRM1-CRM5 conical ridge models are taken as 865 m, 500 m, 290 m, 135 m, 45 m, respectively. So, the shape-ratios for the CRM1-CRM5 models is 1.73, 1.0, 0.58, 0.27 and 0.09, respectively (Table 1). The response of homogeneous half-space is also computed to quantify the conical ridge effects on ground motion characteristics.

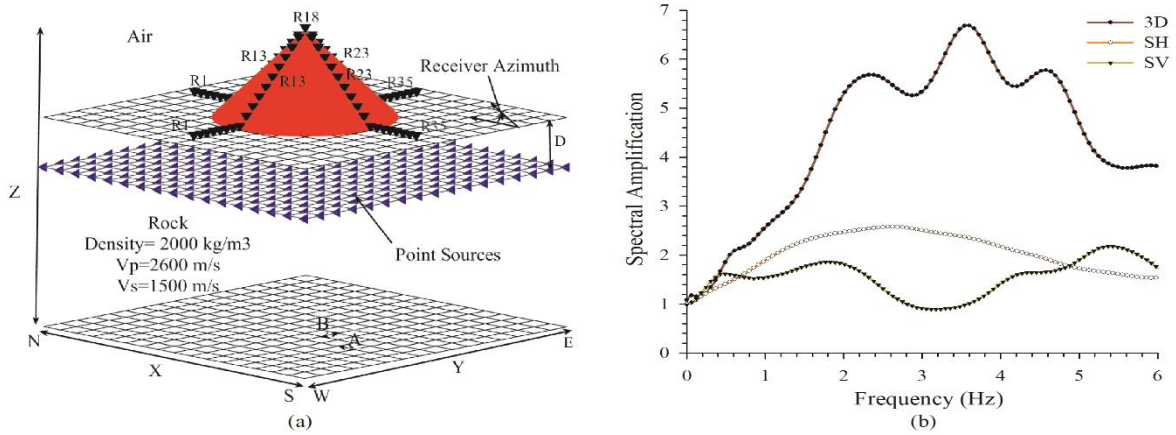

Fig. 1a – Illustrates conical ridge model, NS- and EW-receiver arrays and point sources at a depth 'D' to generate a plane S-wave front propagating vertically upward (Note: X, Y, Z axis's point towards north, east and vertical, respectively), and (b) a comparison of computed spectral amplifications using NS-component of response at the top of 3D conical ridge, the horizontal components of SH- and SV-wave responses at the top of a 2D cross-section of conical ridge in the NS-plane.

Table 1 – The dimension and shape-ratio of different considered conical CRM1-CRM5 ridge models.

Name of models	Height (H) (m)	Width (W)(m)	Shape Ratio (SR)	WA (degree)	Slope (degree)
CRM1	865	1000	1.73	60	60
CRM2	500	1000	1	90	45
CRM3	290	1000	0.58	120	30
CRM4	135	1000	0.27	150	15
CRM5	45	1000	0.09	170	5

2.2 Rheological parameters

The 2D and 3D seismic responses of the ridge models have been computed using fourth-order staggered-grid viscoelastic SH-wave, P-SV wave and 3D finite-difference programs developed by Narayan and co-researchers [14, 15, 16]. Material independent anelastic function was used since it is more suitable for the air-rock discontinuities in the FD grid [16]. The unrelaxed moduli, required input parameters for model, are computed using the P-wave and S-wave velocities and respective quality factors at a reference frequency (ω_r). The P-wave velocity (V_P), S-wave velocity (V_S), P-wave quality factor (Q_P) and S-wave quality factor (Q_S) at the reference frequency (Fr=1.0 Hz), density (ρ) and unrelaxed moduli (unrelaxed Lame's parameters μ_u and γ_u and unrelaxed modulus $K_u = \gamma_u + 2\mu_u$) for the viscoelastic rock and air are given in Table 2. To reduce the requirement of computational time and memory, the ridge models have been discretized with a continuous variable grid size [17]. The grid size in vertical direction is taken as 5 m from top of the model to a depth of 45 m from free surface and 10 m thereafter. The grid size in NS- and EW- directions is taken as 5 m. The time step is chosen to be 0.0005 s to avoid stability problem.

Table 2 – Rheological parameters for the viscoelastic rock and air.

Materials	Velocity and quality factor at F_R				Density (Kg/m^3)	Unrelaxed moduli (GPa)		
	V_P (m/s)	V_S(m/s)	Q_P	Q_S		μ_u	K_u	λ_u
Air	260	0	26	∞	200	0.0	0.0152	0.0152
Rock	2600	1500	260	150	2000	4.589	1.367	4.495

2.3 Source receiver arrays

A plane wave front of S-wave has been generated in FD grid by using so many point sources at a depth of 245 m. A particular point was generated using shear stress in the form of Ricker wavelet. The dominant frequency in the Ricker wavelet was taken as 2.0 Hz with a frequency bandwidth 0-6 Hz. The seismic responses on the NS- and EW-arrays have been computed on 35 receiver points placed horizontally at an equal distance of 50 m extending from 850 m left to 850 m right of ridge axis along the flanks of topography (Fig. 1a). Further, to quantify the dependency of topography effects on azimuth, seismic responses were also computed on various receiver arrays along the topography with different azimuthal plane having azimuth angle between 0 and 180 degrees with respect to north (Note: azimuthal angle of 0 degree corresponds to the NS-array).

2.4 Snapshots of the wave-field

In order to understand the seismic wave behaviour after interaction with the 3D conical ridge topography, snapshots of the wave-field were computed at different moments from 0.26 sec to 2.32 sec and shown in Fig.2. The height and diameter of conical ridge is taken as 1500 m and 3000 m purposely with material properties same as given in Table 2. It can be seen from snapshots that as wave-front moves upwards free surface, it is reflected by ridge topography and it reaches the crest of ridge at time 1.68 sec. The snapshot at time 0.26 sec shows only the incident wave in the considered area. The snapshot at time 0.52 sec shows the incident plane wave front interacting with the conical ridge. It can be seen at time t= 0.61 sec, t=0.81 sec and t=1.26 sec that wave-front is propagating upward. The maximum amplitude is obtained at t=1.68 sec. At t=2.32 sec wave moves out from the conical ridge. But, there are still some seismic phases with opposite polarity in the ridge mass.

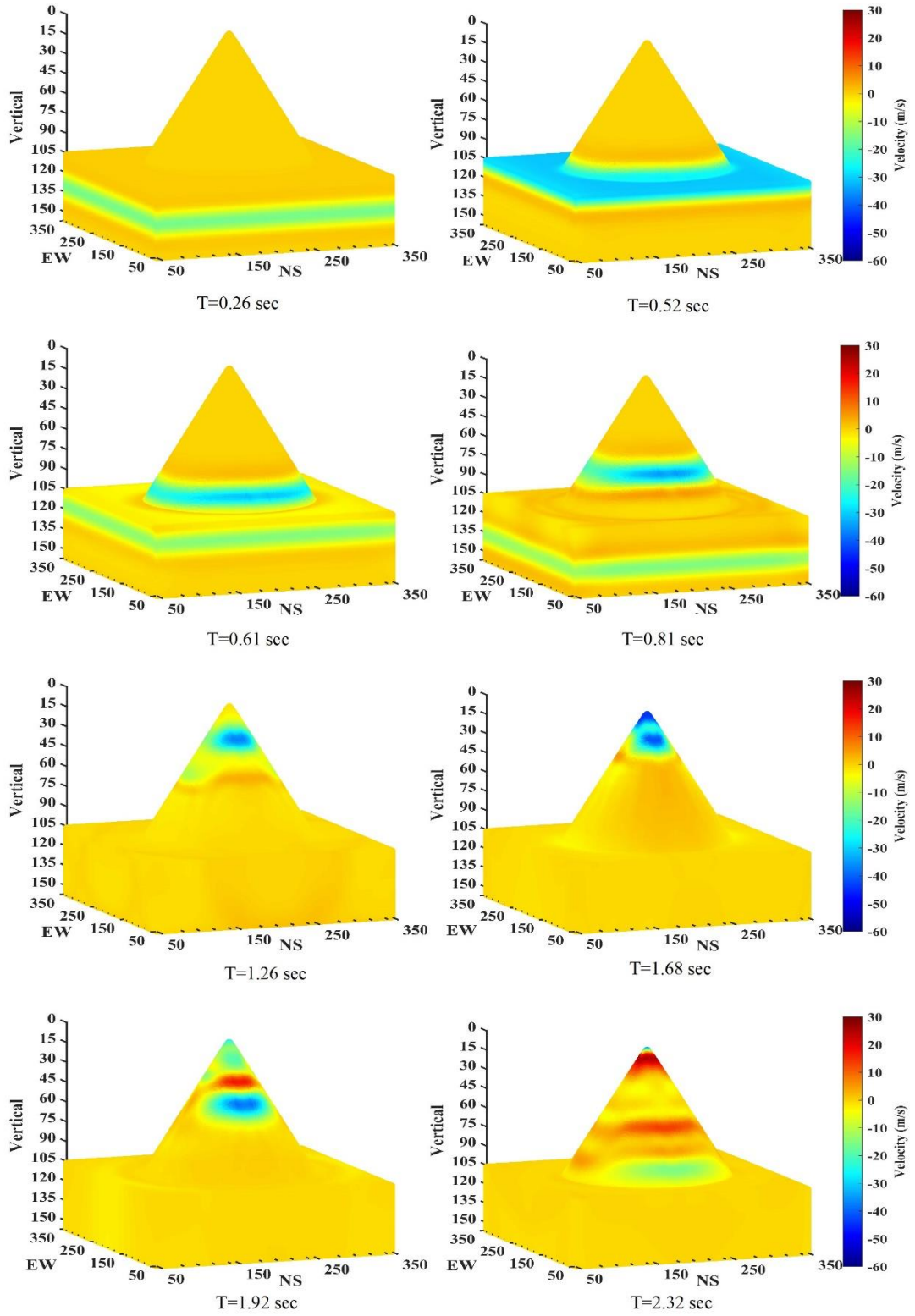

Fig. 2 – Diagram showing the snapshot of seismic wave-field at different moments during its propagation from source to ridge.

3. Effects of shape-ratio of conical ridge

Fig.3 (a-e) shows the NS-, EW- and vertical components of seismic responses of the CRM1-CRM5 conical ridge models along the NS-array, respectively. The seismic waves are recorded only in the NS- and vertical components and not in the EW-component since the particle motion in the incident plane wave front is only in the NS-direction. The analysis of Fig.3 depicts largest amplitude in the NS- component at the ridge top and it is decreasing with the decrease of shape ratio of the conical ridge. In contrast to EW-component, there is some amplitude in the vertical component along the flanks of the ridges due to mode conversion of reflected S-wave from the flanks of ridge as well as due to the diffraction of incident S-wave from the base of the ridge. In other word, the vertically incident S-wave is behaving like SV-wave in the NS-plane. However, amplitude in the vertical component at the top of ridge is zero. A decrease of amplitude amplification at the ridge top with decrease of shape-ratio is inferred.

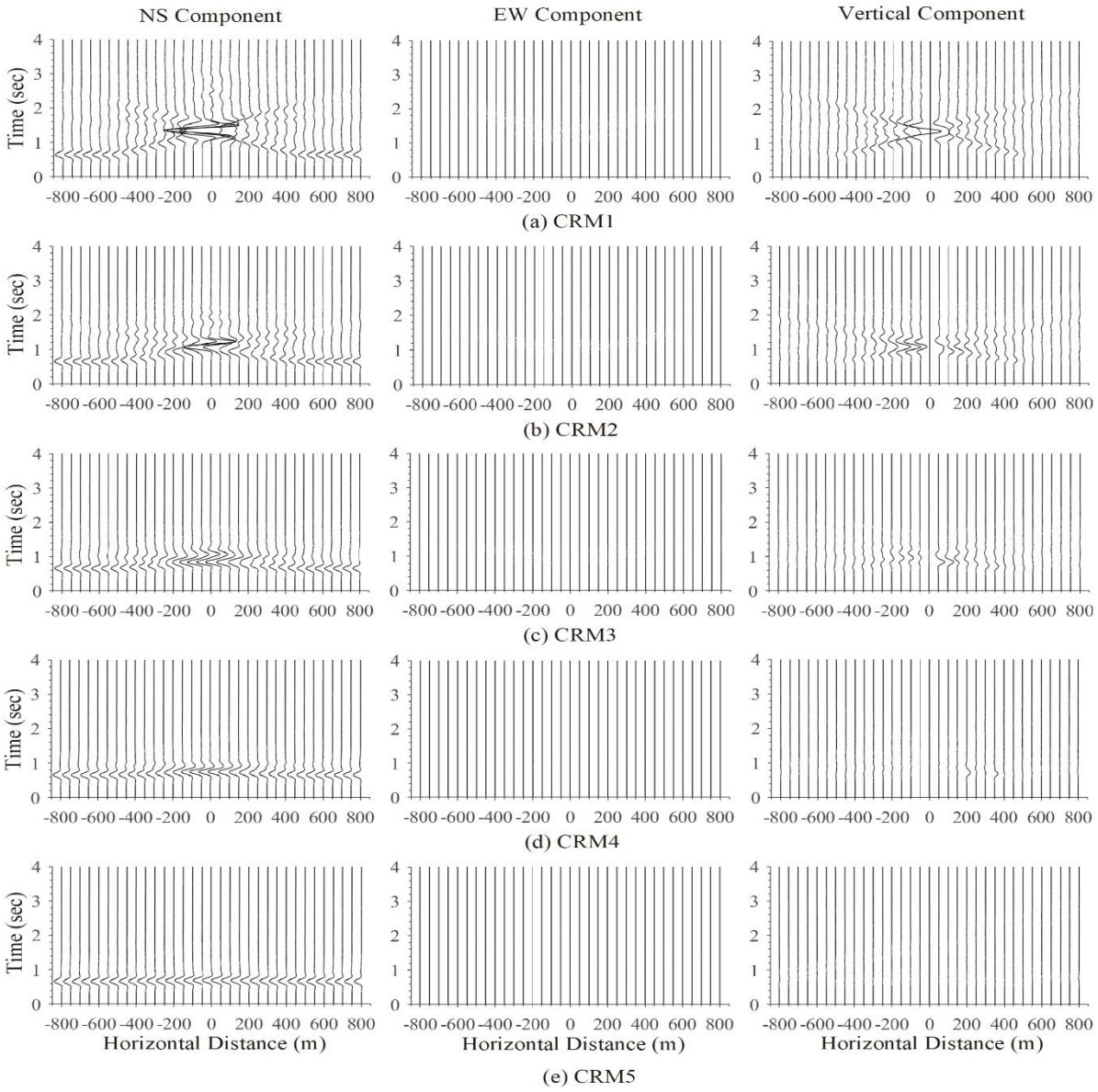

Fig. 3 (a-e) – The NS-, EW- and vertical components of S-wave of responses of the conical CRM1-CRM5 ridge models along the NS-array, respectively (Note. NS-array has azimuth angle 0 degree).

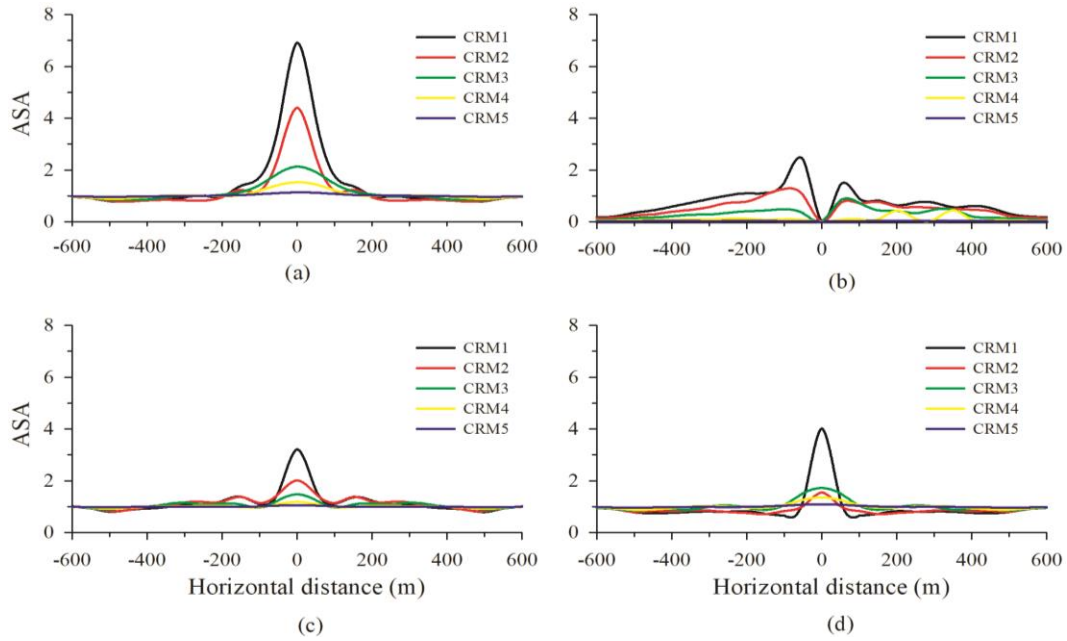

Fig. 4a&b – The obtained ASA in the NS- and vertical components of responses of CRM1-CRM5 models along the NS-array, respectively; (c&d) ASA in the horizontal components of SH- and SV-wave responses of a 2D plane of CRM1-CRM5 ridge models in the NS-direction, respectively.

In order to compared the amplification obtained using 3D simulation with the 2D response, the SH-wave and SV wave response of a plane passing along the NS-array were also computed using a plane wave fronts of SH- and SV-waves. The spectral amplifications at different receiver points due to conical ridge is computed using the ratio of spectra of response of the model for with and without ridge. Figure 1b shows a comparison of spectral amplification at the top of 3D conical ridge with shape-ratio 1.0 with those obtained using SH- and P-SV wave responses. The spectral amplifications in the 3D topography are too large as compared to those obtained in the case of 2D topography. Further, it is larger in the SH-wave response as compared to the SV-wave response. The average spectral amplification (ASA) has been computed using the average of spectral amplifications in the frequency bandwidth of 0-6 Hz. The computed ASA can be used to transfer the peak ground acceleration at the base level of ridge to different locations along the flanks. Fig.4a&b shows the spatial variation of the ASA in the NS-component and vertical-component, respectively. Fig.4c&d shows the comparison of ASA in the horizontal components of SH-wave and SV-wave responses, respectively. The ASA obtained at the top of conical ridge in the NS-component is around 2.2 and 1.7 times larger than that obtained in the SH- and SV-wave responses in the horizontal direction. It is interesting to note that ASA obtained at the top of ridge in the SV-wave response of CRM1 model is more than that obtained in the case of SH-wave response and reverse was the case for rest of the models. A decrease of ASA along the flanks with decrease of SR can be inferred in both 2D and 3D responses of the topography. The obtained 1.7-2.2 times larger ASA in the 3D simulation as compared to 2D simulations calls for the 3D simulation of topography effects. The obtained ASA in the CRM1-CRM5 models reveals that there is no need of computation of topography effect if SR is less than 0.15.

4. Variation of ridge effect with azimuth

In quest of finding the topography effect at all the points on the 3D topography, S-wave responses were computed along different planes using separate receiver array with different azimuth with respect to the true north. The responses of CRM2 conical ridge with shape ratio as 1.0 have been computed and analysed. Fig.5a&b shows the ASA computed along different arrays with azimuthal angles 15 degree to 165 degree for

NS- vertical components, respectively. The ASA variation in the NS-component up to a horizontal distance of 100 m from the ridge axis is unaffected by the change of azimuth of the plane of the receiver arrays, but, ASA in the vertical component is zero at the top of ridge and is increasing up to a distance of around 100 m as well as affected by the azimuth of the recording array. The analysis of Fig.5 also depicts increase of ASA with increase of azimuthal angle of plane of receiver array from 15 to 90 degree from a distance of 100 m to 500 m and thereafter decrease up to azimuthal angle 165 degrees in the NS-component. In contrast to this, in the vertical component, the ASA is continuously decreasing up to azimuthal angle 90 degree and thereafter increasing up to 165 degree. This may be due to the behaviour of the incident S-wave. For example, it was pure SV-wave in the NS-plane (azimuthal angle 0 degree) and purely SH-wave in the EW-plane (azimuthal angle 90 degree). This can be inferred from Fig.5b wherein ASA is zero when azimuth of the receiver array is 90 degrees.

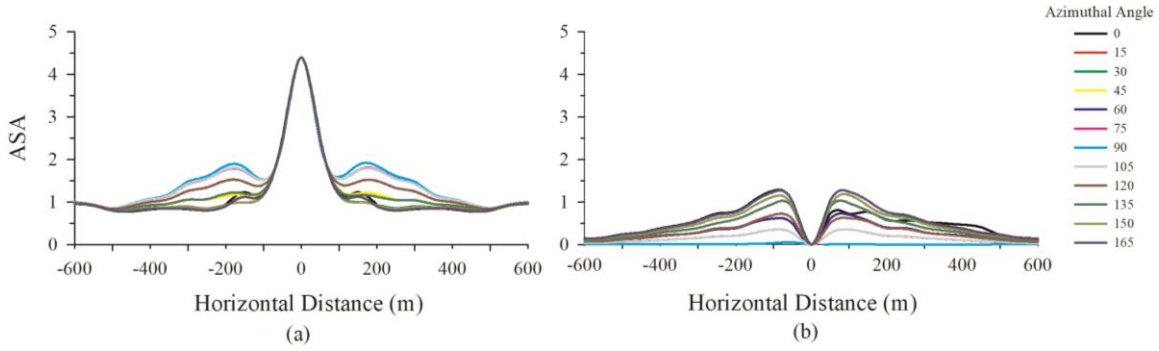

Fig. 5a&b – Comparison of obtained ASA in the NS- and vertical components, respectively along various receiver arrays with different azimuthal angles.

5. Effects of complexity on conical ridge

To understand the effect of geometrical complexity of ridge mass on the ground motion, seismic responses of two complex ridge models namely CR3 and CR5 with shape-ratio 1.0 was computed (Fig. 6). The complexity in the model has been increased by adding the sub-ridges and sub-valley inside the solo- conical topography model, as shown in Fig.1a. The volume of the conical ridge mass is being keep constant while adding the complexity. In CR3 model three sub-ridges and two sub-valleys has been considered and in CR5 model 5-sub-ridges and 3-sub-valleys has been considered (Fig.6). The seismic responses have been recorded on 57 receiver points (25 m apart horizontally), extending from 700 m left to 700 m right of ridge axis along the NS-direction. Fig.7a&b shows the NS-, EW- and vertical components of S-wave responses of CR3 and CR5 models, respectively. The analysis of Fig.7 depicts that the amplitude and duration of ground motion is getting increased with the increase of complexity in the surface geometry. The increase of amplitude in the vertical component with the increase in ridge-complexity can be inferred. The significant amplitude of ground motion at sub-ridges can also be seen. Fig.8a&b shows the comparison of computed ASA for the NS- and vertical components of CR3 and CR5 models, respectively with ASA obtained in the SH-wave and SV-wave responses of the equivalent 2D model. It can be seen that there is increase in amplification with increase in complexity. For example, the obtained maximum ASA in the case of CR5 model as 7.46 is larger than that obtained in the case of CR3 model (4.46). Further, in the case of CR5 model, the largest ASA is obtained at the top of sub-ridges at a distance of 125 m. Furthermore, the computed ASA in the case of 3D topography is much higher than that obtained in the case of equivalent 2D models.

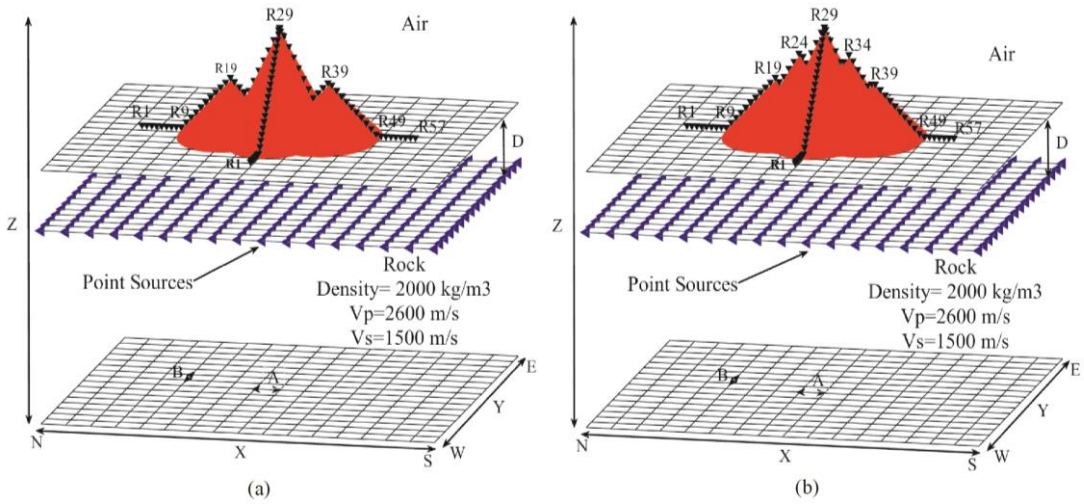

Fig. 6a&b – Sketches for the considered complex conical CR3 and CR5 ridge models, respectively.

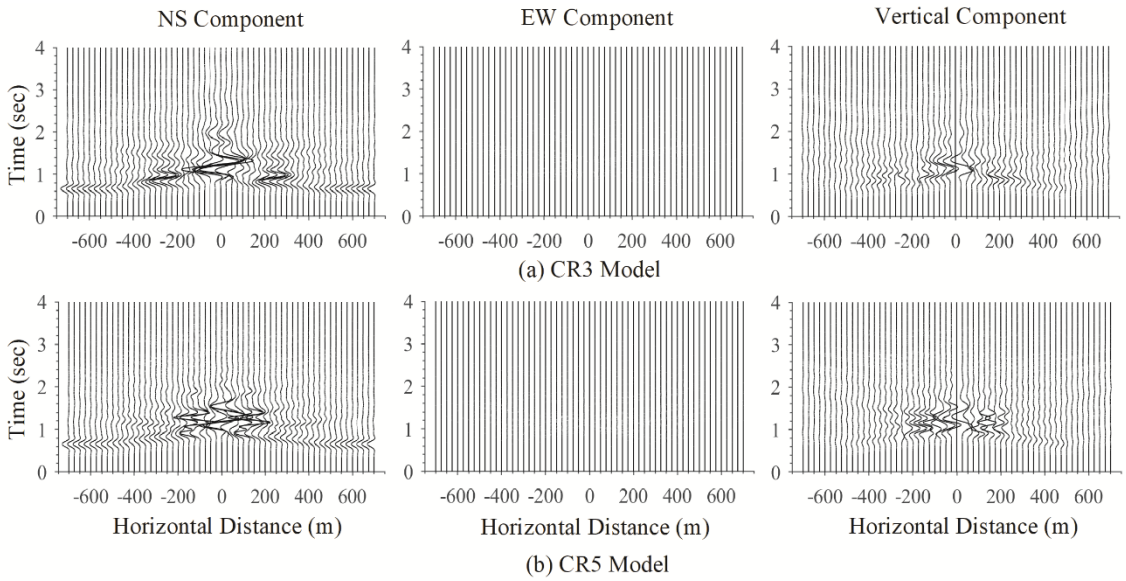

Fig. 7 – S-wave responses of the complex CR3 and CR5 ridge models along the NS-array.

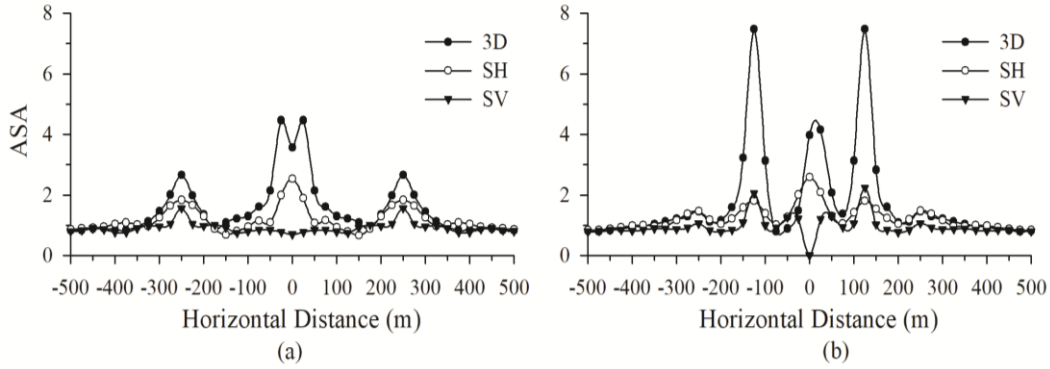

Fig. 8a&b – Comparison of ASA obtained for 3D, SH- and SV-wave horizontal responses in the NS-plane of CR3 and CR5 models, respectively.

6. Ridge amplification using SSR method

To understand the limitations/problems associated with experimental methods for calculation of topography effects, spectral amplifications were computed using the spectral ratio of records at the ridge with the record at the base/near the base of ridge, which is equivalent to use of SSR-method in the case of experimental methods (this approach is mentioned as SSR method in this paper purposely). The SSR-model used to compute the spectral amplifications caused by CMR2 conical ridge with shape ratio1.0. Further, spectral amplifications were also computed by dividing the spectra of 3D response of CRM2 model with the spectra of response in the absence of topography (this approach is mentioned as 3D/1D method purposely in this paper). Fig.9 a&b shows the spectral amplifications computed using SSR method and 3D/1D approach, respectively. The obtained very large amplification at 1.2 Hz as well as relatively larger spectral amplifications in the case of SSR method as compared to 3D/1D approach may be due to the decrease of spectral amplitudes at the base of ridge caused by the diffracted waves. For example, largest spectral amplifications at the top of conical ridge is obtained as 10.4 and 6.7 using SSR method and the 3D/1D approach. Fig.10 shows the comparison of ASA computed using SSR method and 3D/1D approach. This figure clearly depicts 1.3 time larger ASA in the case of SSR method.

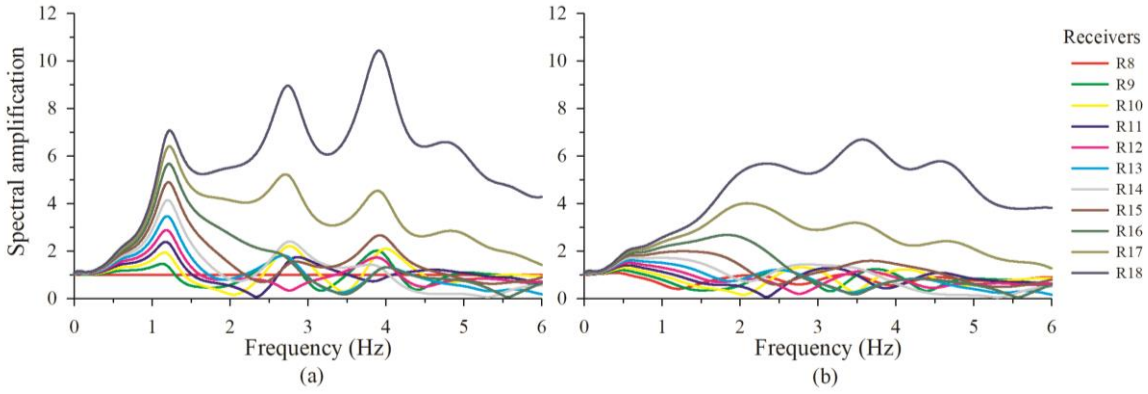

Fig. 9a&b – Computed spectral amplifications in the case of a conical ridge with shape-ratio 1.0 using SSR-method and 3D/1D approach, respectively.

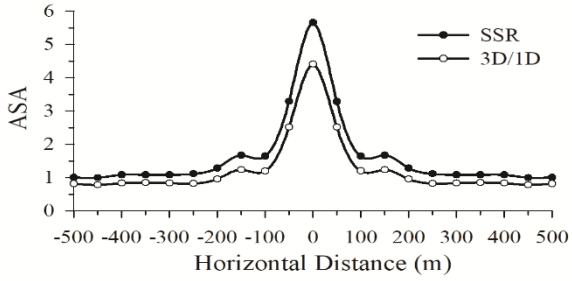

Fig. 10 – Comparison of ASA obtained for conical ridge with shape-ratio 1.0 using SSR-method and 3D/1D approach.

7. Conclusions

The analysis of the 2D and 3D responses of the conical simple and complex topography revealed very large spectral amplifications and ASA in the 3D response as compared to the 2D response. For example, the ASA obtained in the NS-component at the receiver on top of conical ridge with shape ratio 1 and the same computed using SH- and SV wave response of a plane of same conical ridge in NS-direction were 4.4, 2, 1.54 respectively. An increase of both the spectral amplifications and ASA with the increase of shape-ratio is obtained. It is inferred that there is no need of incorporation of topography effect in seismic hazard prediction

on a hill with shape-ratio less than 0.15. The complexity of the conical ridge has caused unexpected larger ASA at the top of side-sub-ridges as compared to the central-sub-ridge. Further, complexity of conical ridge caused maximum ASA of the order of 7.5 which is larger than the same obtained using solo-conical ridge as 4.4. The obtained ASA at the base of sub-valleys more than 1.0 also reflects the need of consideration of complexity of the topography in the numerical simulations. The obtained ASA using SSR method was an overestimation of topography amplification. The observed variation of ASA with the azimuth of the receiver points, particular at a distance more than 100 m, may be due to the change of behaviour of incident S-wave from SV-wave in the NS-plane to SH-wave in the EW-plane and mixed one in between two planes. Based on the simulated results, it is inferred the cause of over prediction of topography effect using SSR method (experimental one) may be the de-amplification of the ground motion at/near the base of the ridge. Finally, it concluded that there is need of consideration of shape, azimuth, complexity and weathering of 3D topography as well as hypo-central distance and focal mechanism of earthquake in numerical estimates of the topography effects on ground motion characteristics.

8. Acknowledgement

The first author is very much thankful to Indian Institute of Technology, Roorkee for providing financial support for presenting this paper in 17WCEE, Japan.

9. References

[1] Boore DM (1972): A note on the effect of simple topography on seismic SH waves. *Bulletin of the seismological society of America*, ***62***(1), 275-284.

[2] Spudich, P., Hellweg, M., & Lee, W. H. K. (1996): Directional topographic site response at Tarzana observed in aftershocks of the 1994 Northridge, California, earthquake: implications for mainshock motions. *Bulletin of the Seismological Society of America*, ***86***(1B), S193-S208.

[3] Massa M, Barani S, Lovati S (2014): Overview of topographic effects based on experimental observations: meaning, causes and possible interpretations. *Geophysical Journal International*, ***197***(3), 1537-1550.

[4] Narayan JP, Kumar V (2015): A numerical study of effects of ridge-weathering and ridge-shape-ratio on the ground motion characteristics. *Journal of Seismology*, ***19***(1), 83-104.

[5] Poursartip B, Fathi A, Kallivokas LF (2017): Seismic wave amplification by topographic features: A parametric study. *Soil Dynamics and Earthquake Engineering*, ***92***, 503-527.

[6] Wang G, Du C, Huang D, Jin F, Koo RC, Kwan JS (2018): Parametric models for 3D topographic amplification of ground motions considering subsurface soils. *Soil Dynamics and Earthquake Engineering*, ***115***, 41-54.

[7] Trifunac MD, Hudson DE (1971): Analysis of the Pacoima dam accelerogram—San Fernando, California, earthquake of 1971. *Bulletin of the seismological Society of America*, ***61***(5), 1393-1411.

[8] Bouchon M, Barker JS (1996): Seismic response of a hill: the example of Tarzana, California. *Bulletin of the Seismological Society of America*, ***86***(1A), 66-72.

[9] Nagashima F, Matsushima S, Kawase H, Sánchez-Sesma FJ, Hayakawa T, Satoh T, Oshima M (2014): Application of horizontal-to-vertical spectral ratios of earthquake ground motions to identify subsurface structures at and around the K-NET site in Tohoku, Japan. *Bulletin of the Seismological Society of America*, ***104***(5), 2288-2302.

[10] Assimaki D, Gazetas G, Kausel E (2005): Effects of local soil conditions on the topographic aggravation of seismic motion: parametric investigation and recorded field evidence from the 1999 Athens earthquake. *Bulletin of the Seismological Society of America*, ***95***(3), 1059-1089.

[11] Geli L, Bard PY, Jullien B (1988): The effect of topography on earthquake ground motion: a review and new results. *Bulletin of the Seismological Society of America*, ***78***(1), 42-63.

[12] Lee SJ, Chan YC, Komatitsch D, Huang BS, Tromp J (2009): Effects of realistic surface topography on seismic ground motion in the Yangminshan region of Taiwan based upon the spectral-element method and LiDAR DTM. *Bulletin of the Seismological Society of America*, ***99***(2A), 681-693.

[13] Dhabu A, Dhanya J, Raghukanth STG (2019): Effect of topography on earthquake ground motions. In *Recent Advances in Structural Engineering, Volume 2* (pp. 107-117). Springer, Singapore.

[14] Narayan JP, Kumar S (2013): A fourth-order accurate finite-difference program for the simulation of SH-wave propagation in heterogeneous viscoelastic medium. *Geofizika*, **30**, 173-189.

[15] Narayan JP, Kumar V (2014): P-SV wave time-domain finite-difference algorithm with realistic damping and a combined study of effects of sediment rheology and basement focusing. *Acta Geophysica*, **62(3),** 1214-1245.

[16] Narayan JP, Sahar D (2014): Three-dimensional viscoelastic finite-difference code and modelling of basement focusing effects on ground motion characteristics. *Computational Geosciences*, ***18***(6), 1023-1047.

[17] Narayan JP, Kumar S (2008): A fourth order accurate SH-wave staggered grid finite-difference algorithm with variable grid size and VGR-stress imaging technique. *Pure and Applied Geophysics*, ***165***(2), 271-294.

